The electrochemical oxidation of organics using tungsten oxide based electrodes

Bock, Christina; MacDougall, Barry

Publisher's version / Version de l'éditeur:
http://dx.doi.org/10.1016/S0013-4686(02)00273-6
Electrochimica Acta, 47, 20, pp. 3361-3373, 2002

PERGAMON

Electrochimica Acta 47 (2002) 3361–3373

ELECTROCHIMICA Acta

www.elsevier.com/locate/electacta

The electrochemical oxidation of organics using tungsten oxide based electrodes

C. Bock *, B. MacDougall

Institute for Chemical Process and Environ. Tech., National Research Council of Canada, Montreal Road, Ottawa, ON, Canada K1A 0R6

Received 16 January 2002; received in revised form 15 April 2002

Abstract

High surface area tungsten oxide (WO_x) based electrodes containing centers of Pt, Sn or Ru were synthesized. The WO_x electrodes were found to display good capacitive behavior and relatively high specific capacitance values of up to 180 F g^{-1}. The oxidation behavior of particularly HCOOH and $(COOH)_2$, using the WO_x electrodes containing Pt and Sn centers (Pt/WO_x and Sn/WO_x, respectively), was studied in detail in aqueous solutions at high potentials, i.e. at which O_2 is evolved. Both HCOOH and $(COOH)_2$ appear to be oxidized following 1st order kinetics. The $(COOH)_2$ oxidation reaction is faster than the HCOOH reaction using otherwise the same experimental conditions. The reaction mechanism of both the HCOOH and $(COOH)_2$ oxidation was found to most likely involve the adsorptive interaction of the two organics with the anode surface. The WO_x based anodes appear to be promising catalysts for the anodic oxidation of both $(COOH)_2$ and HCOOH.

Keywords: Tungsten oxide films; Oxidation of organics; Capacitance; Anodic oxidation mechanism; Pt, Sn and Ru 'dopants'

1. Introduction

Tungsten oxides (WO_x) have attracted much attention due to their use in electrochromic devices, their electrocatalytic properties and their potential use as sensors for pH measurements [1–3]. They are also of practical interest due to their chemical inertness, particularly in acidic solutions [4]. A range of methods can be used to prepare WO_x such as cathode sputtering, vacuum evaporation, pyrolytic spray deposition and sol–gel techniques [5–7]. It has been established that WO_x prepared using expensive vacuum evaporation methods show the most promising properties needed for practical applications. More recently, it has also been shown that WO_x films of promising properties can be deposited electrochemically. Kulesza and Faulkner [8] deposited non-stoichiometric WO_x containing Pt microcenters onto various conducting substrates from acidified Na_2WO_4 solutions employing a continuous potential cycling method, while Shen and Tseung [9,10] deposited WO_x films at constant negative potentials. Both groups incorporated microcenters of foreign elements (namely Ni, Fe and Pt) into the oxide films via electrochemical co-deposition. Tungsten oxide films showing rapid faradaic film conversion reactions were formed in this manner. Tseung et al. deposited the oxide films using a solution of peroxotungstic acid, formed by the dissolution of metallic tungsten powder with hydrogen peroxide. They suggested that peroxotungstic acid is deposited onto the conductive substrate in the form of an inorganic oxide polymer. Hydrous WO_x films of high porosity on the micrometer scale were formed in this manner [10]. X-ray diffraction studies suggested the WO_x to be amorphous [10].

The faradaic WO_x film oxidation and reduction reactions are accompanied by a film color change from blue to transparent, and from transparent to blue, respectively. In acidic solutions, the faradaic film conversion reaction is believed to involve the formation of tungsten bronzes (H_xWO_3), as follows [11]:

$$WO_3 + xH^+ + xe^- = H_xWO_3 \quad (1)$$

This reaction (Eq. (1)) suggests that protons are expelled from the oxide film during oxidation in acidic solutions, and vice versa, they are injected into the oxide film

* Corresponding author. Tel.: +1-613-9902252; fax: +1-613-9412529

E-mail address: christina.bock@nrc.ca (C. Bock).

0013-4686/02/$ - see front matter
PII: S0013-4686(02)00273-6

during reduction, thus maintaining electroneutrality within the film. The involvement of protons in the oxide film conversion reaction is consistent with the experimentally observed shift in the WO_x oxidation/reduction peak with solution pH of close to -60 mV pH^{-1} (an apparent Nernstian behavior) versus a pH independent electrode [10]. The electrocatalytic properties of WO_x films, particularly of films containing Pt microcenters, have also been studied. Kulesza and Faulkner [12] investigated the electro-reduction of bromate to bromide using these oxide film electrodes, while Shen and Tseung [10] reported that such oxide films show good catalytic properties for the methanol oxidation reaction.

In this work, WO_x films containing foreign elements (namely Pt, Ru and Sn) are deposited at constant negative potentials and the films are characterized using electrochemical methods. In particular, current–potential curves of these oxide films are analyzed to obtain the capacitive film responses and the kinetics of the faradaic film conversion reactions are briefly discussed. The performance of these oxide films towards the oxidation of organic compounds is investigated in some detail. The oxidation reactions of a range of organics (such as formic, acetic and oxalic acids, as well as alcohols such as isopropanol and *t*-butanol) are investigated over a broad potential range, i.e. at potentials more negative and more positive than needed for the evolution of O_2 (oer).

2. Experimental

2.1. Electrochemical formation of WO_x containing Pt, Ru or Sn

Tungsten oxides containing foreign elements such as Pt, Ru and Sn (and referred to as Pt/WO_x, Ru/WO_x and Sn/WO_x, respectively) were formed electrochemically by applying a constant negative potential (E_{d-}) for up to 120 min using a method similar to that described by Shen and Tseung [9,10]. To our knowledge it is the first time that Ru and Sn is being incorporated into these WO_x films. Immediately prior to the deposition (i.e. the application of E_{d-}), the potential was held at 0 V versus saturated calomel electrode (SCE) for 30 s allowing the system to equilibrate. The oxide films were deposited from a 0.1 M tungsten solution (see below) containing either 8 mM H_2PtCl_6 (Alfa Aesar, 99.9% metals basis), 8 mM $RuCl_3$ (Alfa Aesar, 99.99% metals basis) or ca. 8×10^{-2} mM saturated $SnCl_2$ (Alfa Aesar, 98% metals basis). The WO_x films were deposited onto IrO_2 coated Ti substrates (Alfa Aesar, 99.7% metals basis) that are referred to as Ti/IrO_2 substrates. The IrO_2 coating was formed by the thermal decomposition (at 500 °C) of a 0.14 M $IrCl_4$ EtOH solution. The $IrCl_4$ solution was painted onto the Ti substrates using a brush. This procedure (painting and decomposition) was repeated twice resulting in ca. 150 nm thick IrO_2 layers, as estimated in prior work [13]. Immediately prior to the formation of the IrO_2 layer, the Ti substrates were mechanically polished using sandpaper, ultrasonically cleaned in EtOH, etched in boiling (80 °C) 10 M HCl for 10 min, and then well rinsed with high resistivity water. It is known that W oxide films can be deposited onto a variety of conductive substrates [8,11]. In this work, the oxide films were deposited onto Ti/IrO_2 substrates, as it is well known that the lifetime of oxide anodes is enhanced in this manner [14].

The 0.1 M tungsten solution was prepared by slowly dissolving 9.1925 g W-powder (1–5 micron, Alfa Aesar, 99.9% metals basis) in 60 cm^3 H_2O_2 (30%, Anachemia). The excess H_2O_2 was decomposed by immersing a high surface area Pt gauze into the solution at open circuit. Afterwards, 150 cm^3 EtOH was added and the solution was finally diluted to 500 cm^3 with water.

2.2. Cells and electrodes

A three compartment cell, in which the reference electrode was separated from the working electrode compartment by a Luggin capillary, was generally employed for the electrochemical studies. However, for the anodic oxidation of the model organic compounds, an H-cell was used allowing the separation of the working and counter electrodes using a Nafion@ 117 membrane (DuPont). The period of the anodic electrolysis was generally short (<12 h) in order to avoid cross-over of the organics from the working to the counter electrode compartment. Either a SCE or a mercury sulfate electrode (MSE: +0.435 V vs. SCE) was used as reference electrode. In all organic oxidation studies, the MSE was used to avoid Cl^- contamination. All potentials reported in this paper are versus the SCE unless otherwise stated. A large surface area Pt gauze served as the counter electrode. In some cases, a polycrystalline Pt foil (0.1 mm thick, 99.99% metals basis, Alfa Aesar) was also employed as working electrode. The geometrical area of all working electrodes employed was 0.98 cm^2 and electrode areas are referred to as geometrical unless otherwise stated.

2.3. Techniques and instrumentation

Electrochemical experiments were performed using either an EG&G 273 potentiostat or a Solartron SI 1287 electrochemical interface (Solartron Group, Ltd.) both driven by Corrware software program (Scribner, Assoc.). Ohmic drop compensation was performed when necessary, i.e. for experiments involving high currents using either a 'feedback' or 'sampled' mode. The concentration of the organic species were determined using a HP series 1100 high performance liquid chro-

matograph (HPLC). An Ion-Interaction column (Mandel), thermostated at 46 °C, was used. The UV detector was set at 195 nm. Sulfuric acid (0.01 M) was used as mobile phase at a flow rate of 0.3 cm^3 min^{-1}. A Shimadzu UV-1201 S UV/Vis Spectrophotometer was used to identify possible organic reaction products. A Mitutoyo micrometer was used for the measurement of the oxide film thickness. The amount of oxide deposited was roughly estimated using a Mettler Toledo AB 54 balance. For the CO_2 estimations, the electrolysis cell was tightly sealed using RTV 2 silicon rubber adhesive sealant and the CO_2 produced during the electrolysis was captured in 0.01 M NaOH. Sulfuric acid was added to adjust the pH of the NaOH capturing solution to ca. 3. Immediately afterwards, the CO_2 concentration was measured using an accumet CO_2 gas sensing ion selective electrode.

2.4. Solutions

Oxidation studies were performed using appropriate concentrations of $(COOH)_2$, HCOOH and CH_3COOH as well as isopropanol, *t*-butanol and MeOH in 0.5 M H_2SO_4. Anodic electrolysis studies were carried out using 20 cm^3 of solution containing the organic compound of interest unless otherwise stated. High resistivity (18 MΩ) water and A.C.S. grade chemicals were used. High purity Ar gas was used to deoxygenate the electrolyte solution and the electrochemical experiments were performed at room temperature. During electrochemical experiments, the solutions were either 'quiet' or rapidly stirred using a magnetic stirring bar for solution agitation, as indicated in the text.

3. Results and discussion

3.1. Electrochemistry and electrochemical formation of WO_x films

3.1.1. WO_x film deposition

The amount of WO_x film deposited was found to depend on the E_{d-} value employed to form the oxide and to be different for the three solutions used in this work. An E_{d-} value of −0.65 V was used for the deposition of the Pt/WO_x and Sn/WO_x films, while the Ru/WO_x films were deposited at −1.4 V. These particular E_{d-} values were used because preliminary studies showed that they resulted in approximately the same amounts of WO_x being deposited during 120 min from the solutions containing Pt, Ru or Sn. Fig. 1 shows current density–time (J–t) curves recorded for the deposition of Pt/WO_x, Ru/WO_x and Sn/WO_x films. All three films were deposited for 120 min. It is seen that the cathodic current density, and hence the charges (173 C (Ru/WO_x), 117 C (Pt/WO_x) and 58 C (Sn/WO_x)) are

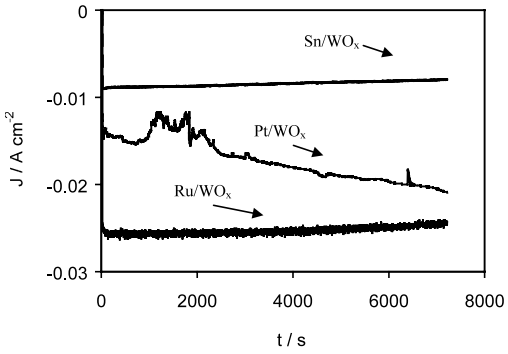

Fig. 1. Current density–time curves for the deposition of Pt/WO_x, Sn/WO_x and Ru/WO_x films onto Ti/IrO_2 substrates from 'quiet' solutions. The following potentials for the oxide deposition were used: −0.65 V for the Pt/WO_x and Sn/WO_x films and −1.4 V for the Ru/WO_x film vs. SCE.

different for the deposition of the three films, in spite of the fact that similar amounts of oxides (ca. 5×10^{-3} g) were formed in the three cases. This is related to the fact that hydrogen is also evolved during the oxide deposition process, resulting in a decrease in current efficiency for the oxide film formation. The extent of the H_2 evolution reaction (her) is likely to influence the porosity of the films. The her takes place to different extends depending on the identity of the foreign element, as well as the potential of the deposition (i.e. case of Ru).

3.1.2. Electrochemical characteristics of WO_x films

Fig. 2a–c show typical slow sweep CVs (2 mV s^{-1}) for the Pt/WO_x, Ru/WO_x and Sn/WO_x films recorded in 0.5 M H_2SO_4. Steady-state CVs were obtained within the 2nd cycle. The electrochemical conversion of the Sn/WO_x and Ru/WO_x films results in a broad oxidation/reduction J–E profile between ca. −0.3 and 0.3 V rather than the well defined oxidation/reduction peaks observed for films deposited from acidic Na_2WO_3 solutions by E-cycling [8]. In fact, the J–E curve for the oxidation/reduction of particularly the Sn/WO_x film shows good capacitive behavior, as seen in the close to rectangular J–E curve (i.e. $dJ/dE \approx$ zero). Kulesza and Faulkner [8] observed similar oxidation/reduction J–E curves for the electrochemical conversion of the Pt/WO_x films in K_2SO_4 solutions. They suggested this behavior to be due to the high concentration of potassium ions that presumably hinder the reductive formation reaction of tungsten bronze, H_xWO_3, that requires protons (Eq. (1)). According to them, the WO_x film reduction takes place according to the reaction shown in Eq. (2) [8]:

$$WO_3 + 2yH^+ + 2ye^- = WO_{3-y} + yH_2O \quad (2)$$

The absence of well defined WO_x oxidation/reduction peaks for the Ru/WO_x and Sn/WO_x films studied here may indicate that these films are also converted according to Eq. (2), as opposed to Eq. (1), i.e. that the formation of H_xWO_3 is hindered by the presence of Sn

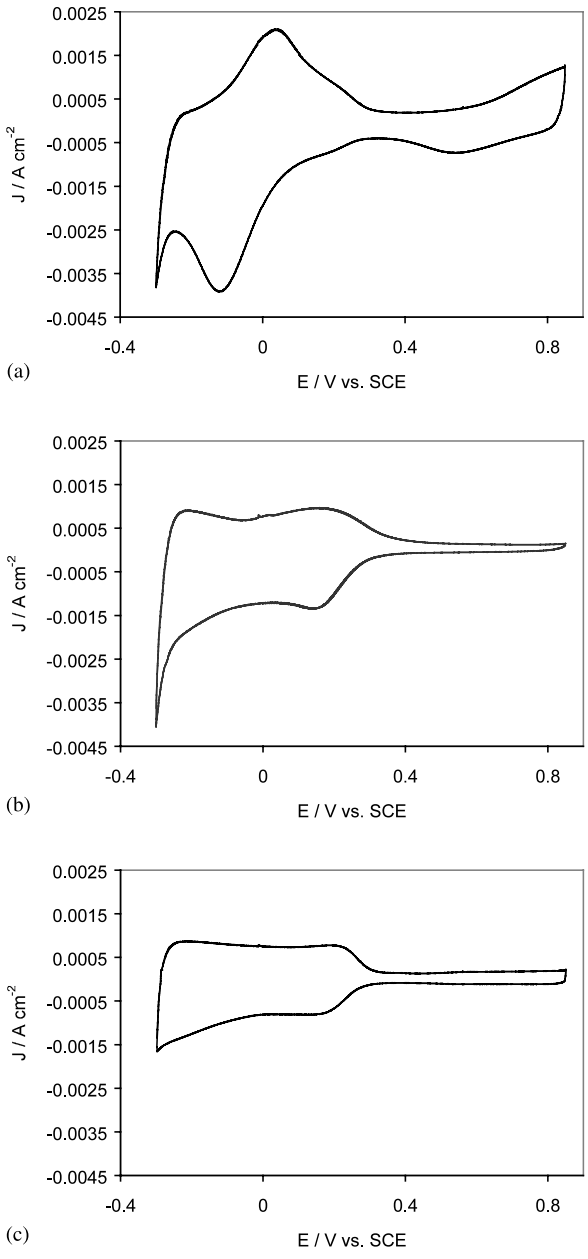

Fig. 2. (a–c) Typical CVs for Pt/WO_x (a), Ru/WO_x (b), Sn/WO_x (c) films recorded at 2 mV s^{-1} in 0.5 M H_2SO_4 under 'quiet' conditions. The films were deposited onto Ti/IrO_2 substrates for 120 min. The Pt/WO_x and Sn/WO_x films were deposited at 0.65 V, while the Ru/WO_x film was deposited at 1.4 V. An SCE was employed for the deposition and the CV experiments.

and Ru within the film. Since elucidating the exact conversion reaction mechanism was not the primary goal of this research, no further work was carried out along this line.

Characteristics typical for the Pt electrochemistry are recognizable in the CV response for Pt/WO_x. Between −0.25 and 0.3 V, the adsorption/desorption reaction of atomic hydrogen [10] takes place on Pt film sites. Therefore, the Pt/WO_x films do not show the close to ideal capacitive response observed for the Sn/WO_x and Ru/WO_x films. At more positive potentials (positive cycle at above 0.6 V and negative cycle between ca. 0.8 and 0.4 V), the oxidation of Pt to Pt-oxide is seen to take place, and during the cathodic sweep the reduction peak typical for the conversion of Pt-oxide to Pt is clearly visible [15]. The characteristics for the Ru conversion reaction (likely seen within ca. 0 and 0.4 V) for the Ru/WO_x film (Fig. 2b) are less defined than for the Pt/WO_x film (Fig. 2a). Ru has multiple oxidation states and its CV characteristics are generally known to be broad, i.e. the oxidation/reduction peaks are not well defined [16]. Fig. 3 shows typical plots for the film charge density (Q_{WO_x}) for Pt/WO_x and Sn/WO_x versus the log of the sweep rate (v). Films of ca. 30 and 100 μm (film thickness measured in the dry state using a micrometer) were deposited for 30 and 120 min, respectively. The Q_{WO_x} values are equivalent to half of the complete oxidation and reduction charge passed in the CVs between −0.26 and 0.3 V for the Pt/WO_x and −0.3 and 0.3 V for the Sn/WO_x films. It is seen that below a critical sweep rate (which depends on the film composition and deposition time), Q_{WO_x} reaches a maximal value that is independent of the sweep rate for a particular WO_x film. This indicates that at v's slower than a critical value all electro-active sites within the WO_x films have time to react, and hence, the complete film charge is recovered. The sweep rate that allows complete film charge recovery is, therefore, referred to as the equilibrium sweep rate (v_{eq}) and yields a measurement of the charge transfer kinetics of these oxide films, as has been similarly discussed for related systems [15,16]. It is seen (Fig. 3) that the v_{eq} values are different for these four films. In fact, v_{eq} values of ca. 10 mV s^{-1} are found for the Pt/WO_x and Sn/WO_x films deposited for 30 min, while v_{eq} values of ca. 2 mV s^{-1} are found for the Pt/WO_x and Sn/WO_x films deposited

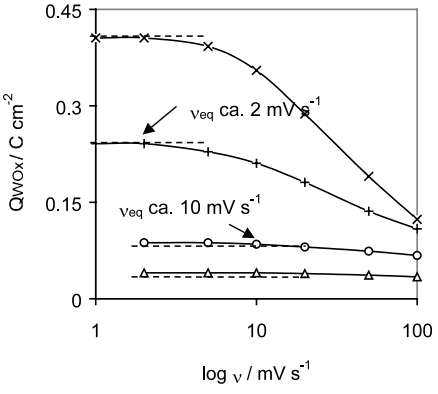

Fig. 3. Q_{WO_x} dependence on the log(v) for Pt/WO_x and Sn/WO_x films. The Q_{WO_x} values are extracted from experimental CV data recorded in 0.5 M H_2SO_4 under 'quiet' conditions. (x) shows the Q_{WO_x} values for a Pt/WO_x film deposited for 120 min, (+) shows the same, but for a Sn/WO_x film deposited for 120 min, (○) shows the Q_{WO_x} data for a Pt/WO_x film deposited for 30 min and (Δ) shows the data for a Sn/WO_x film deposited for 30 min.

for 120 min. This indicates that more time is needed for all electro-active film sites to react for thicker oxide films. This is consistent with prior work [17,18] that has shown that the time needed for complete charge recovery for inorganic oxide films and conductive polymers increases with increasing film thickness.

The capacitance of the WO_x films (C_{WO_x}) was calculated by dividing the Q_{WO_x} value extracted from experimental slow sweep ($v \leq v_{eq}$) CV data, by 0.56 V for the Pt/WO_x film and 0.6 V for the Ru/WO_x and Sn/WO_x films. The C_{WO_x} values were further divided by the weight of the corresponding oxide film, and multiplied by the surface area of the film, thus yielding the specific capacitance (C_{sp,WO_x}). Reasonably high C_{sp,WO_x} values of ca. 180 F g^{-1} for the Pt/WO_x and ca. 100 F g^{-1} for the Ru/WO_x and Sn/WO_x films were estimated. These C_{sp,WO_x} values are comparable to values reported for carbon based double layer capacitors and capacitors based on conductive polymers of 10–100 and 100–200 F g^{-1}, respectively [16]. The larger C_{sp,WO_x} value found in this work for the Pt/WO_x, in comparison with the Ru/WO_x and Sn/WO_x films, is due to the hydrogen adsorption/desorption at Pt film sites that also contributes to the film capacitance.

3.2. Oxidation characteristics for organic's using Pt/WO_x and Sn/WO_x anodes

In the following sections, the oxidation of aliphatic carboxylic acids and alcohols using Pt/WO_x and Sn/WO_x anodes is investigated. The WO_x films used in the following sections were generally deposited for 120 min. 'Simple' organic compounds are used in this work with the goal of better understanding the mechanism of their anodic oxidation. Aromatic compounds such as phenol and *p*-benzoquinone have often been used in prior studies [19–23]. However, the reaction mechanisms of these compounds is rather complex, involving consecutive and parallel reaction pathways, and therefore are not deemed appropriate for investigating the role of catalyst composition in organic electro-oxidation reactions [21,23]. Before and after the oxidation studies, equilibrium CVs ($v < v_{eq}$) were recorded to confirm that the electrochemical properties of these films were not altered during these anodic oxidation studies. Furthermore, Ru/WO_x anodes, while interesting from the viewpoint of deposition and redox characteristics, were not used in these studies due to the instability of Ru in acidic solutions at positive potentials.

3.2.1. Equilibration of Pt/WO_x and Sn/WO_x anodes

The influence of anodic electrolysis on the stability and J–E characteristics of Pt/WO_x and Sn/WO_x films was first investigated. Fig. 4a and b show typical CVs for Pt/WO_x and Sn/WO_x films, respectively, deposited for 120 min and recorded in 0.5 M H_2SO_4 before and

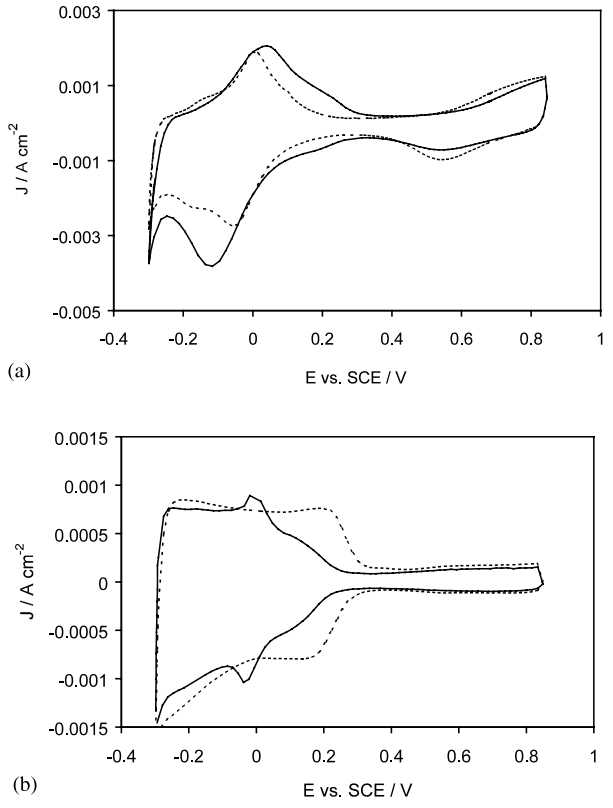

Fig. 4. (a and b) Typical CVs for Pt/WO_x (a) and Sn/WO_x (b) films deposited for 120 min and recorded at 2 mV s^{-1} in 0.5 M H_2SO_4 under 'quiet' conditions. The CVs for the films before (—) and after 7 days (----) of anodic electrolysis at 10 mA cm^{-2} in 2 M H_2SO_4 under 'quiet' conditions are shown.

after 7 days of electrolysis at constant anodic current density (10 mA cm^{-2}) in 2 M H_2SO_4. The CV characteristics of the Pt/WO_x and Sn/WO_x films are seen to be clearly altered as a result of the electrolysis, while no changes in oxide film mass were detected (within $\pm$0.2 mg). The PtO reduction charge is seen to increase as a result of the electrolysis, indicating an increase in the electro-active Pt surface area. This, and the fact that the oxide film mass appears to be constant, suggests that a large number of Pt sites within the unused WO_x films are not accessible for the H_2SO_4 electrolyte solution prior to the electrolysis treatment. The fact that the electro-active Pt surface area increases during constant-current electrolysis likely suggests that either Pt migrates to film sites that are more accessible for the H_2SO_4 electrolyte solution or there is an opening up of the film structure. After ca. 4 days of electrolysis at 10 mA cm^{-2} in 2 M H_2SO_4, steady-state CVs were obtained for both the Pt/WO_x and Sn/WO_x film electrodes, indicating that changes within the film induced by the electrolysis conditions have been completed. Therefore, the Pt/WO_x and Sn/WO_x films were equilibrated in 2 M H_2SO_4 at 10 mA cm^{-2} for 7 days prior to their use as anodes in the oxidation studies of organics discussed below.

3.2.2. Oxidation characteristics for organics at low potentials in quiet solutions

The oxidation characteristics of a range of organics were studied in a potential region (generally between −0.3 and 1.1 V) where significant O_2 evolution is not observed. Polycrystalline Pt was also used as an electrode and the experimental data are summarized in Table 1 for solutions of 0.5 M of a particular organic compound (0.1 M for $(COOH)_2$) in 0.5 M H_2SO_4. It is seen that all organics tested in this work are readily oxidized (showing clearly defined oxidation characteristics in the raw CV data) using Pt/WO_x and polycrystalline Pt except for CH_3COOH, while only the $(COOH)_2$ oxidation characteristics are observed using Sn/WO_x anodes. Furthermore, the $(COOH)_2$ oxidation peak potential is more positive using the Sn/WO_x than the Pt/WO_x and Pt electrodes suggesting that the $(COOH)_2$ oxidation is facilitated using Pt/WO_x and Pt electrodes. The fact that CH_3COOH is not oxidized is not unexpected, as it is well known that this particular compound is difficult to oxidize under these conditions. Furthermore, for the same organic compound very similar oxidation potentials are found for the Pt/WO_x and Pt electrode. These results suggest that the organics are oxidized at the Pt film sites, and that the role of the WO_x in the organic oxidation reaction is to serve as a conductive, high surface area support for the Pt sites. For the Pt/WO_x electrode, the electro-active Pt area was calculated from the PtO reduction peak. To do this, the potential was cycled at $v < v_{eq}$ to 1.09 V in 0.5 M H_2SO_4 and a value of 420 μC cm^{-2} [22] was used to convert the PtO reduction charge to the electro-active Pt surface area. Electro-active Pt surface areas for the (0.98 cm^2 geometrical area) Pt/WO_x films were calculated to be between 95 and 340 cm^2 suggesting roughness factors of between 100 and 350. For both the Pt/WO_x and Pt electrodes, the peak currents depend strongly on the type of organic as indicated in Table 2. It should be noted that the concentration of the organic was always 0.5 M, with the exception of $(COOH)_2$ where it was 0.1 M. The lower concentration in the case of $(COOH)_2$ was necessary because of the high anodic currents associated with this organic. The oxidation peak current observed for a particular organic compound using a 95 or 340 cm^2 (real Pt surface area) Pt/WO_x electrode was divided by the peak current observed for the same compound, but using a 1.05 cm^2 (real surface area) Pt electrode. This yields the ratio of the oxidation peak current for the Pt/WO_x versus the Pt electrode; the peak currents were extracted from the raw CV data at 10 mV s^{-1}. For the case of $(COOH)_2$ oxidation, the ratio of the oxidation peak currents is close to one as opposed to the 340 ratio expected if all the WO_x Pt sites could be used for the organic oxidation reaction. This means that, effectively, the extent of Pt utilization in the Pt/WO_x is particularly poor for $(COOH)_2$ oxidation carried out under these conditions. In the case of $(CH_3)_3COH$, the ratio of 91 is very close to the theoretical value; for $(CH_3)_2CHOH$, it is between 15 and 25% of the theoretical value, depending on the Pt/WO_x surface area. The incomplete utilization of Pt sites could simply be due to mass transport limitations of the organics into the high surface area, porous structure of the Pt/WO_x film. This explanation is consistent with the fact that the anodic activity of the Pt electrode is highest with $(COOH)_2$, i.e. any substantial increase in current, due to a roughness increase, will run into problems with the rate of supply of reactant, $(COOH)_2$, to the same geometrical area. This arises because the diffusion layer thickness, under the un-stirred conditions employed here, is much greater than the 'scale of roughness' of the Pt/WO_x deposit film. In the case of *t*-butyl alcohol, there is no such problem since the reaction is much slower and entirely under activation control. For the other organics examined, the reaction is probably under 'mixed' mass transport and activation control with a corresponding 'mixed' result.

Table 1
Oxidation characteristics [a] for a range of organics in 'quiet' 0.5 M H_2SO_4 using Pt/WO_x, Sn/WO_x and polycrystalline Pt electrodes

Organic compound	E_{pa} vs. SCE (V)		
	Pt/WO_x	Sn/WO_x	Polycrystalline Pt
0.5 M HCOOH	0.65 [b]	No oxidation peak	0.6 [b]
0.5 M CH_3COOH	No oxidation peak	No oxidation peak	No oxidation peak
0.1 M $(COOH)_2$ [c]	0.78	1.1	0.78
0.5 M $(CH_3)_2CHOH$	0.32	No oxidation peak	0.32
0.5 M $(CH_3)_3COH$	0.9	No oxidation peak	0.9
0.5 M CH_3OH	0.6	No oxidation peak	0.6

[a] The oxidation characteristics are extracted from experimental CVs recorded between −0.3 and 1.1 V vs. SCE at 10 mV s^{-1}. The data are corrected for IR drop using IR interruption for experiments involving high currents.
[b] Oxidation peaks at 0.3 and 1.25 V were also observed for HCOOH oxidation using Pt/WO_x and polycrystalline Pt electrodes.
[c] 0.1 M instead of 0.5 M $(COOH)_2$ solutions were used, as discussed in the text.

3.2.3. 'Anodic' oxidation of model organics

In this section, the anodic electrolysis of *t*-butanol as well as HCOOH, $(COOH)_2$ and CH_3COOH was investigated using Pt/WO_x and Sn/WO_x anodes at potentials above the oer and with solution stirring. Either 'high' anodic currents or sufficiently positive potentials (thus allowing the oer to take place) were employed. The oxidation of organics carried out in this manner is referred to as 'anodic oxidation' in this work. This

Table 2
Oxidation currents for a range of organics in 'quiet' 0.5 M H_2SO_4 estimated from CV studies using Pt/WO_x and polycrystalline Pt electrodes

	i_{pa} (A) [a]for 1.05 cm^2 Pt electrode	i_{pa} (A) [a] for Pt/WO_x electrode	Electro-active Pt area for Pt/WO_x electrode (cm^2) [b]	i_{pa} ratio Pt/WO_x vs. Pt electrode [c]
0.1 M $(COOH)_2$	2.46×10^{-2}	2.48×10^{-2}	340	1.01
0.5 M CH_3OH	1.77×10^{-3}	2.81×10^{-1}	340	158.8
0.5 M $(CH_3)_2CHOH$	1.56×10^{-3}	6.26×10^{-2}	340	40.1
0.5 M HCOOH	7.51×10^{-4}	1.05×10^{-1}	340	139.8
0.5 M $(CH_3)_3COH$	2.36×10^{-5}	2.15×10^{-3}	95	91

[a] Magnitude for the anodic current peak maxima (i_{pa}) for a particular organic (as indicated in column 1) and 0.5 M H_2SO_4. The i_{pa} values were estimated from slow sweep CV experiments between 0.3 and 1.1 V recorded at 10 mV s^{-1}.

[b] The electro-active Pt area was estimated from the PtO reduction charge passed in a slow sweep CV experiments recorded in 0.5 M H_2SO_4, as discussed in the text. The potential was cycled between −0.3 and 1.09 V.

[c] i_{pa} ratio equals the experimentally observed i_{pa} value for the oxidation of a particular organic using the Pt/WO_x electrode divided by the i_{pa} value observed using the polycrystalline Pt electrode.

'anodic oxidation' process has attracted much attention in recent years, due to its potential use for the removal of toxic organics from waste-water [13,19–21]. In prior work, it has been suggested that the organic compounds (R) can be oxidized to CO_2 via hydroxy radicals formed as intermediate products at the anode oxide surface (MO_x) during the oer, as follows [19]:

$$MO_x + H_2O \rightarrow MO_x(^{\bullet}OH) + H^+ + e^- \quad (3)$$

$$MO_x(^{\bullet}OH) \rightarrow MO_{x+1} + H^+ + e^- \quad (4)$$

$$MO_{x+1} \rightarrow MO_x + 1/2O_2 \quad (5)$$

$$MO_x(^{\bullet}OH)_z + R \rightarrow MO_x + CO_2 + zH^+ + ze^- \quad (6)$$

It should be noted that the actual mechanism of the oer depends on the anode composition, and hence could be somewhat different from the reactions suggested in Eqs. (3)–(5). In an alternative reaction scheme, it has been suggested that pre-adsorption of organics on specific surface sites of the anode is a key factor responsible for increased efficiencies of the anodic oxidation process [21]. There is still some controversy about the oxidative removal of organic compounds using metal oxide anodes and clarification of the reaction mechanism is needed. In order to evaluate the potential use of the WO_x based anodes made in this work for the oxidation of organic compounds, as well as to gain insight into the mechanism of these anodic oxidation processes, systematic studies using simple organic compounds were carried out, as discussed below. It is noteworthy that organics such as $(COOH)_2$ are considered to be difficult to oxidize due to their high activation energy [19,20]. In fact, in prior studies, correlations between the hydroxy concentration on an anode surface and the oxidizability of $(COOH)_2$ have been made using different anode materials [19].

Fig. 5a and b show typical plots for the concentration dependence of HCOOH and $(COOH)_2$, respectively, on the electrolysis time (t) for anodic electrolysis carried out at a constant potential of 1.335 V using a (285 cm^2 real Pt area) Pt/WO_x anode, while Fig. 5c and d show the same, but plotting $\ln(c_0/c_{(t)})$ versus the electrolysis time (t). The initial concentration (c_0) was 8×10^{-4} and 10^{-3} M of HCOOH and $(COOH)_2$, respectively and $c_{(t)}$ is the concentration of HCOOH or $(COOH)_2$ found at a particular electrolysis time. For these particular electrolysis experiments, 14 and 20 cm^3 of solutions were used for the HCOOH and the $(COOH)_2$ oxidation, respectively and the data shown in Fig. 5a–d were corrected for changes in the volume occurring as a result of withdrawing samples in 200 μl portions for the HPLC analyzes. The experimental HCOOH and $(COOH)_2$ electrolysis data suggest that the anodic oxidation of these two organics follows 1st order reaction kinetics. This is indicated by the fact that the dependence of the experimental $c_{(t)}$ data on the electrolysis time can be described using an exponential relationship shown in Fig. 5a and b. This is also supported by the fact that $\ln(c_0/c_{(t)})$ follows a linear relationship with the electrolysis time passing through zero origin. This allows the extraction of the 1st order rate constant (k_1) from the slope of this plot, as indicated in Fig. 5c and d [23]. The results could also be interpreted in terms of a mass transport controlled process operating at the limiting current, which would itself be dependent on the organic's concentration. Indeed, in 'quiet solutions' during cyclic voltammetry, the $(COOH)_2$ oxidation does appear to be under mass transport control (seen in Table 2). However, in the present situation, the solutions are under strong mechanical stirring, and the oxidation rate constants are independent of the solution stirring rate. It could be argued that parallel oxygen evolution causes the mass transport control to be masked since it causes solution agitation on its own, which overrides the 'forced' solution agitation. However, the fact that additional experiments under conditions where little or no O_2 evolution occurs gave similar results, adds support to the 'activation-control' mechanism [24]. The fact is that the operating potential in the

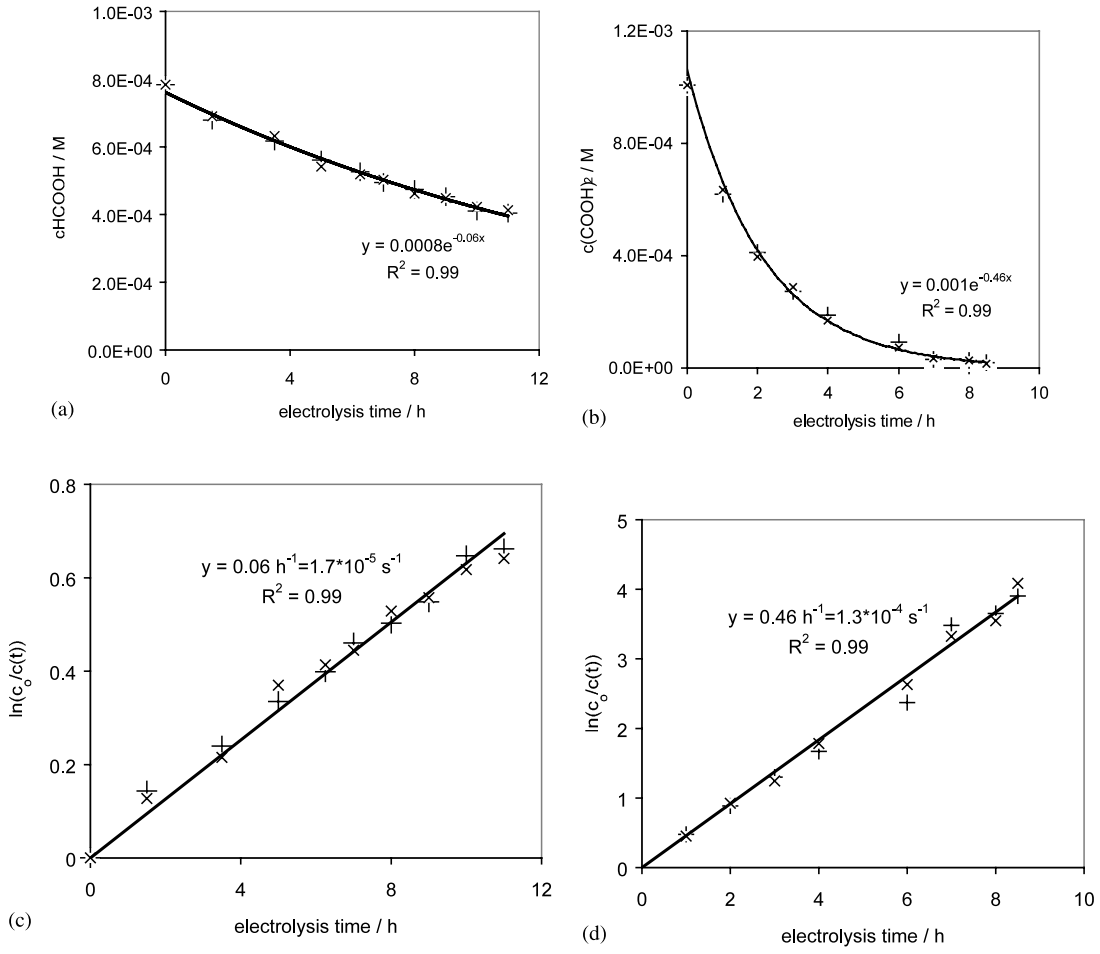

Fig. 5. (a–d) Typical concentration ($c_{(t)}$) vs. time curves for the electrolysis of 14 cm^3 of initially 8×10^{-4} M HCOOH (a) and 20 cm^3 of 10^{-3} M $(COOH)_2$ (b) in 0.5 M H_2SO_4. (+) and (x) represent the data for two consecutive carried out electrolysis experiments. A 285 cm^2 real Pt area Pt/WO_x anode of 0.98 cm^2 geometrical area was used. (c and d) show the $\ln(c_0/c_{(t)})$ vs. time plots for the HCOOH and $(COOH)_2$ electrolysis experiments, respectively using the data shown in (a and b). The solid lines in (a and b) represent the best fit to the experimental data using an exponential relationship between $c(t)$ and the electrolysis time. The solid lines in (c and d) show the same, but using a linear relationship of $\ln(c_0/c_{(t)})$ vs. t. The electrolysis experiments were carried out at 1.335 V vs. SCE, however, an MSE was employed in the actual experiment. All solutions were mechanically stirred.

present experiments is in the highly anodic region where the rate of $(COOH)_2$ oxidation is lower (in comparison to the 'cyclic volammetry at low potentials' situation), and probably well below the limiting current. More will be said about the details of this experimental analysis in a parallel paper [24]. In the present work, it was found that both HCOOH and $(COOH)_2$ are anodically oxidized following kinetics qualitatively identical as shown in Fig. 5a–d (i.e. suggesting 1st order reaction kinetics). The rate constants indicated in Fig. 5c and d, namely 1.7×10^{-5} and 1.3×10^{-4} s^{-1} for the 14 cm^3 HCOOH and 20 cm^3 $(COOH)_2$ solutions, respectively, also indicate that the HCOOH oxidation is much slower than the $(COOH)_2$ oxidation reaction. In fact, throughout this work, it was found that the anodic HCOOH oxidation reaction is at least five times slower than the $(COOH)_2$ oxidation reaction for a particular WO_x based anode. It is noteworthy that the HCOOH and $(COOH)_2$ oxidation rate constants were up to several orders of magnitude higher than found for Pt as well as antimony doped tin oxide anodes [24], thus indicating the good catalytic activity of these WO_x based anodes for the oxidation of these two organics at higher anodic potentials.

Experiments to determine k_1 values were also performed galvanostatically, at a constant current density of 10 mA cm^{-2} using Pt/WO_x and Sn/WO_x anodes. This results in potentials of ca. 1.3–1.5 V for the particular electrodes used in the galvanostatic experiments carried out here. Again, anodes of 0.98 cm^2 geometrical area were employed and the solutions were rigorously stirred. (As was the case with the potentiostatic experiments, the oxidation reactions studied galvanostatically were most likely not mass transport limited, since the experimental k_1 values were found to be independent of the stirring rate.) The k_1 values

determined galvanostatically for HCOOH and $(COOH)_2$ are in good agreement with those obtained potentiostatically, indicating that either approach can be used with a good degree of confidence under the conditions employed here. Table 3 summarizes the results for all four organics studied here at both Pt/WO_x and Sn/WO_x anodes. A real surface area of 95 cm^2 was estimated for the Pt/WO_x anode. It is seen that HCOOH and $(COOH)_2$ are anodically oxidized using either Pt/WO_x or Sn/WO_x anodes, unlike the results found for the oxidation studies below the oer. Both HCOOH and $(COOH)_2$ are mainly oxidized to CO_2, as shown in Table 4a and b, respectively. This is also supported by the fact that no solution products and no evidence for electrode fouling was found during long term electrolysis studies provided sufficiently high potentials/currents were employed (see below). However, neither CH_3COOH nor *t*-butanol are oxidized (at least at an appreciable rate) using these oxide anodes, as indicated by the fact that their concentration remained constant over long (up to 24 h) electrolysis periods. These observations, and the fact that it has been shown that $(CH_3)_3COH$ and CH_3COOH react using $^{\bullet}OH$ generated using UV methods [25], may indicate that the $^{\bullet}OH$ concentration on these WO_x based anodes is small and/or that the $^{\bullet}OH$ formed in solution and at the surface display different reactivity's. The fact that these two organics are oxidized at lower potentials (see CV studies) may indicate different oxidation mechanism for low and high potentials. It is also seen that the k_1 values for the $(COOH)_2$ oxidation is larger than for the HCOOH oxidation. This indicates that the anodic oxidation of $(COOH)_2$ is more facile and rapid than the HCOOH oxidation, consistent with the results from potentiostatic experiments both above and below the oer. Parallel studies have shown that organics such as methanol and valeric acid are anodically oxidized using Pt/WO_x and Sn/WO_x anodes [24], demonstrating the possible potential use of these anodes for the anodic oxidation of a range of organics.

Table 3
Oxidation rate constants (k_1) for a range of organics in 'mechanically stirred' 0.5 M H_2SO_4 using Pt/WO_x and Sn/WO_x electrodes

Organic compound	k_1 [a] (s^{-1})	
	Pt/WO_x anode	Sn/WO_x anode
HCOOH	2.5×10^{-5}	5.4×10^{-6}
CH_3COOH	0 [b]	0 [b]
$(COOH)_2$	2.1×10^{-4}	2.2×10^{-5}
$(CH_3)_3COH$	0 [b]	0 [b]

[a] 1st order reaction rate constant (k_1) values are extracted from experimental $\ln(c_0/c_{(t)})$ vs. t plots. The anodic oxidation of the organics was carried out at 10 mA cm^{-2} using 0.98 cm^2 (geometrical area) anodes and 20 cm^3 of initially 10^{-3} M solutions of the organic of interest.

[b] No changes in the organic concentration were observed even over long electrolysis periods of 24 h.

The k_1 values for a particular electrode using the same experimental conditions were found to be very reproducible (±10%) and no changes in the CV characteristics of the WO_x based electrodes recorded in 0.5 M H_2SO_4 were detected as a result of the oxidation studies carried out here. However, different k_1 values were found for different Pt/WO_x and Sn/WO_x, anodes. This, and the fact that for the same current the monitored potentials are also different for different Pt/WO_x as well as Sn/WO_x anodes, indicates differences in the number of electro-active sites of these WO_x anodes. These differences are likely due to the nature of the anode catalyst being highly sensitive to the details of the preparation method.

3.2.3.1. Constant E electrolysis experiments using Pt/WO_x anodes at higher potentials.

3.2.3.1.1. HCOOH oxidation. Fig. 6 shows typical current density (J)–time plots for two different HCOOH concentrations in 0.5 M H_2SO_4 (10^{-2} and 10^{-3} M HCOOH), as well as the background, recorded at 1.285 V. A 200 cm^2 real Pt area Pt/WO_x anode was used in the experiments discussed in this section unless otherwise noted. The plots are the average of three to four runs, with reproducibility from run to run being ± 10%. It is interesting to note that the same 'background' in the J–t profile is obtained even immediately after the Pt/WO_x electrode has been used in 10^{-2} M HCOOH, with no intermediate special cleaning, indicating that no electrode poisoning due to e.g. strong organic adsorption on the electrode surface, takes place under these conditions. For similar experiments carried out at 1.385 V, the current was observed to slowly increase with time over an extended HCOOH electrolysis period (> several hours), i.e. as the HCOOH solution concentration decreased. The reversal of direction of current change indicates that the HCOOH oxidation reaction does not result in irreversible blocking of the Pt/WO_x anode surface. It is also seen (Fig. 6) that an increase in the HCOOH concentration clearly decreases the magnitude of J. In fact, a decrease of J with increasing HCOOH concentration was observed for different potentials above 1.2 V, as summarized in Table 5. This behavior strongly suggests that HCOOH undergoes adsorptive interactions with the anode surface as shown e.g. in Eq. (7):

$$MO_x + HCOOH \rightarrow MO_x(COOH)_{ads} + H^+ + e^- \quad (7)$$

However, the adsorbed form of HCOOH does not result in irreversible surface poisoning, as discussed above. The experimental current efficiencies (I_{eff}) for the HCOOH oxidation reaction are very low (Table 5, column 6), indicating that the majority of the monitored current is due to the oer. Fig. 6 also shows that pseudo

Table 4
CO_2 estimation for HCOOH (a) and $(COOH)_2$ (b) electrolysis in 'mechanically stirred' solutions using Pt/WO_x anodes

Electrolysis time (h)	Experimental Δc HCOOH [a] (mol dm^{-3})	Theoretical Δc CO_2 [b] (mol dm^{-3})	Experimental Δc CO_2 [c] (mol dm^{-3})
0–4	$2.7 (\pm 0.4) \times 10^{-4}$	$2.7 (\pm 0.4) \times 10^{-4}$	$2 (\pm 0.8) \times 10^{-4}$
4–7	$6 (\pm 0.4) \times 10^{-5}$	$6 (\pm 0.4) \times 10^{-5}$	$4 (\pm 1) \times 10^{-5}$
Electrolysis time (h)	Experimental Δc $(COOH)_2$ [a] (mol dm^{-3})	Theoretical Δc CO_2 [b] (mol dm^{-3})	Experimental Δc CO_2 [c] (mol dm^{-3})
0–2	$6 (\pm 0.3) \times 10^{-4}$	$1.2 (\pm 0.06) \times 10^{-3}$	$1.1 (\pm 0.05) \times 10^{-3}$
2–4	$2.4 (\pm 0.3) \times 10^{-4}$	$4.8 (\pm 0.6) \times 10^{-4}$	$4.1 (\pm 0.8) \times 10^{-4}$
4–7	$9 (\pm 0.3) \times 10^{-5}$	$1.8 (\pm 0.6) \times 10^{-4}$	$2 (\pm 1) \times 10^{-4}$

[a] Experimental differences in HCOOH and $(COOH)_2$ concentration observed over a specific electrolysis time indicated in column 1. The anodic electrolysis of the organic was carried out at 10 mA cm^{-2} using a 0.98 cm^2 (geometrical area) Pt/WO_x anode and 20 cm^3 of initially 10^{-3} M HCOOH and 10^{-3} M $(COOH)_2$ in 0.5 M H_2SO_4.
[b] Theoretical mol amount of CO_2 formed for 1 dm^3 electrolysis solution calculated from the experimentally observed differences in the HCOOH and $(COOH)_2$ concentrations shown in column 2, assuming that 1 mol HCOOH yields 1 mol CO_2 and 1 mol $(COOH)_2$ yields 2 mol CO_2.
[c] Experimentally found mol amount of CO_2 for 1 dm^3 electrolysis solution.

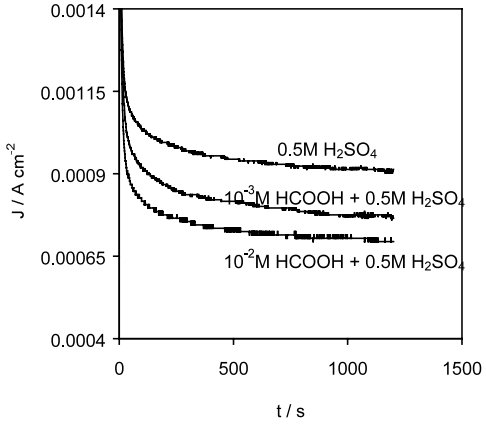

Fig. 6. $J-t$ plots for the anodic electrolysis of 0.5 M H_2SO_4, 10^{-3} M HCOOH+0.5 M H_2SO_4, 10^{-2} M HCOOH+0.5 M H_2SO_4 using a 200 cm^2 real Pt area Pt/WO_x anode of 0.98 cm^2 geometrical area. The electrolysis was carried out at 1.285 V vs. SCE, however, an MSE was employed in the actual experiment. Each curve shown in this figure is the average of three $J-t$ curves recorded for a particular HCOOH concentration. All solutions were mechanically stirred.

steady-state $J-t$ profiles are reached in both the 10^{-3} and 10^{-2} M HCOOH solutions after ca. 10 min. This suggests that for a particular HCOOH concentration, the Pt/WO_x surface is covered with a specific fraction of the adsorbed form of the HCOOH within 10 min. The surface coverage of the adsorbed form of HCOOH onto the Pt/WO_x anode (θ) can be estimated from the pseudo steady-state $J-t$ profiles, using the following relationship:

$$\theta = \frac{J_{0.5\ \mathrm{M}\ H_2SO_4} - J_{\mathrm{HCOOH}}}{J_{0.5\ \mathrm{M}\ H_2SO_4}} \quad (8)$$

This calculation is based on the observation that the majority of the anodic current is due to oxygen evolution as opposed to organic oxidation. In Eq. (8), $J_{0.5\ \mathrm{M}\ H_2SO_4}$ stands for the experimentally observed current densities in the organic free 0.5 M H_2SO_4, while J_{HCOOH} stands for the current density in the presence of either 10^{-3} or 10^{-2} M HCOOH. The θ values calculated using experimental J values obtained after 20 min of electrolysis at a constant potential and a

Table 5
Characteristics for the anodic HCOOH oxidation carried out at different potentials in 'mechanically stirred' solutions using Pt/WO_x anodes

E vs. SCE [a] (V)	$(J_{10^{-3}\ \mathrm{M\ HCOOH}}/J_{0.5\ \mathrm{M}\ H_2SO_4})$ [b]	$(J_{10^{-2}\ \mathrm{M\ HCOOH}}/J_{0.5\ \mathrm{M}\ H_2SO_4})$ [b]	θ [c] for 10^{-3} M HCOOH	θ [c] for 10^{-2} M HCOOH	I_{eff} [d] (%) c_0: 10^{-3} M HCOOH
1.135	1.6	4.6	–	–	190
1.235	0.92	0.78	0.08	0.22	1.4
1.285	0.85	0.76	0.15	0.24	1
1.335	0.84	0.77	0.16	0.23	0.75
1.385	0.88	0.85	0.12	0.15	n.a. [e]
1.435	0.89	0.83	0.11	0.17	0.4

[a] The E values are recorded vs. an SCE, however, an MSE was used for the electrolysis experiments.
[b] The J values are extracted from experimental $J-t$ curves after 20 min of electrolysis at a particular potential. In all cases, the J value reached a pseudo steady-state within less than 20 min of electrolysis.
[c] The θ values are calculated from the experimental pseudo steady-state J values and using Eq. (8).
[d] The I_{eff} values are calculated from HCOOH concentration changes observed during the anodic electrolysis carried out at a particular potential and using Eq. (9). The I_{eff} values reported in column 6 are for the HCOOH concentration change of initially 10^{-3}–7.5×10^{-4} M.
[e] Data not available, as experiment has not been carried out.

particular HCOOH concentration are summarized in Table 5. The results indicate only slight variations of the θ value with potential, while the θ value is clearly influenced by the HCOOH concentration. The θ values of 0.08–0.24 (Table 5) suggest that a significant fraction of the anode surface (ca. 10–25%) active for the oer is covered with the adsorbed form of HCOOH.

Current efficiency (I_{eff}) values for the HCOOH oxidation are also shown in Table 5. The I_{eff} values were calculated by dividing the theoretical charge needed to oxidize 25% of the initially 10^{-3} M HCOOH to presumably CO_2 ($Q_{th(organic \rightarrow CO_2)}$) with the experimental charge passed in the particular anodic electrolysis experiment (Q_{exp}), i.e.

$$I_{eff} = 100 \times \frac{Q_{th(organic \rightarrow CO_2)}}{Q_{exp}} \quad (9)$$

The $Q_{th(organic \rightarrow CO_2)}$ values were calculated using experimentally observed HCOOH concentration changes. The I_{eff} values are seen to be small (1.4% and less) for potentials more positive than 1.235 V and to decrease slightly with increasingly positive potentials. The latter indicates that an increasingly larger fraction of the current is used for the oer than for the HCOOH oxidation, as the potential is made more positive. For lower electrolysis potentials (≤ 1.135 V), I_{eff} values (calculated assuming a $2e^-$ reaction, HCOOH oxidation to CO_2) of more than 100% (in fact close to 200%) were found. This indicates that HCOOH is not oxidized to CO_2 under these conditions, i.e. at potentials that are also more negative than employed for the CO_2 measurements discussed above. It is likely that the anodic HCOOH electrolysis at these low potentials results in a less than $2e^-$ reaction, e.g. only the adsorption reaction of HCOOH onto the anode surface. Anodic HCOOH electrolysis experiments carried out at these potentials were found to decrease the electrode activity for the oer and HCOOH oxidation in subsequent oxidation studies involving fresh solutions. This suggests that the HCOOH electrolysis carried out at 1.135 V resulted in the almost exclusive formation of a poisoning (surface blocking) product that was, however, found to be removable by extensive electrolysis in organic free H_2SO_4 solutions at sufficiently positive potentials (> 1.3 V).

Fig. 7 shows the k_1 values for the HCOOH oxidation as a function of the applied potential; while only four data points are used, it can be seen that a simple relationship between k_1 and the potential does not exist. It appears that k_1 and θ (Table 5) are more closely related, as in fact they show the same dependence on the applied potential with a maximum at ca. 1.335 V. The results obtained in this work suggest that the anodic HCOOH oxidation rate is influenced by the HCOOH solution concentration as well as the fraction of the

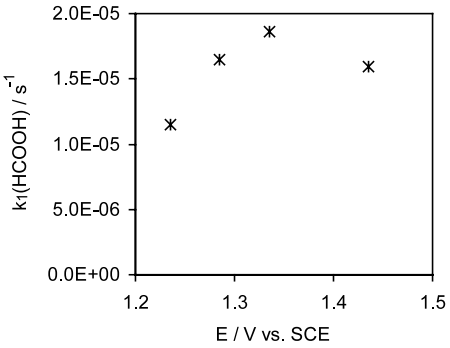

Fig. 7. Experimental k_1 values for the oxidation of originally 10^{-3} M HCOOH + 0.5 M H_2SO_4 as a function of the applied potential. The k_1 values are extracted from experimental $\ln(c_0/c_{(t)})$ vs. time curves. A 200 cm^2 real Pt area Pt/WO_x anode of 0.98 cm^2 geometrical area was used for the electrolysis. The solution was mechanically stirred.

adsorbed form of HCOOH, i.e. the θ value rather than the applied potential. To further investigate this concentration effect (previously shown in Fig. 6), experiments were performed at 1.385 V using a 11 cm^2 real Pt area Pt/WO_x anode in 0.5 M H_2SO_4 with the progressive addition of HCOOH until a 1 M concentration was reached. The results are shown in Fig. 8. (Similar observations are obtained using a 200 cm^2 real Pt area Pt/WO_x anode.) With the addition of HCOOH, the anodic current initially decreases and continues to do so until 5×10^{-2} M HCOOH, after which the current begins to increase. The maximum suppression of the current is found at 5×10^{-2} M HCOOH, for which a θ value of 0.35 is calculated from the experimental current data (note that this calculation assumes that the majority of the observed anodic current is due to O_2 evolution). At HCOOH concentrations higher than 5×10^{-2} M, the measured anodic current increases with increasing concentration, and a plot of the anodic current (without background correction) against

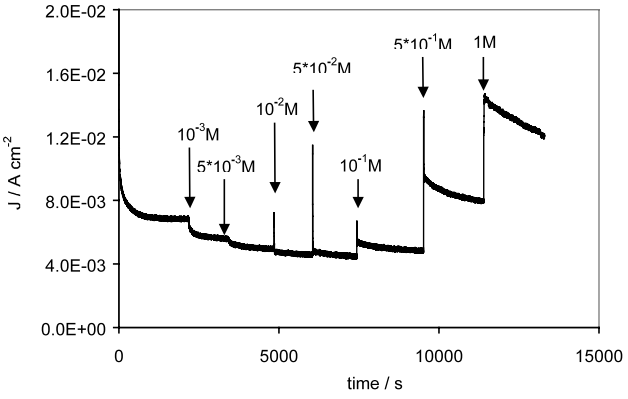

Fig. 8. $J-t$ curves for a 11 cm^2 real Pt area Pt/WO_x anode of 0.98 cm^2 geometrical area in 0.5 M H_2SO_4 and different concentrations of HCOOH, as indicated in the plot. The experiment was carried out at 1.385 V vs. SCE starting with 100 cm^3 of an organic free H_2SO_4 solutions. The mechanically stirred solution was spiked with appropriate amounts of HCOOH during the electrolysis.

HCOOH concentration suggest a 1st order dependence. It is clear that the catalytic activity of the WO_x based anode towards the HCOOH oxidation reaction increases markedly as higher HCOOH concentrations are used. It should, however, be noted that the HCOOH oxidation reaction carried out for high HCOOH concentrations at least partly results in the blocking of the anode surface. This is indicated in the continuous decrease in the current density with time clearly seen for the high HCOOH concentrations (Fig. 8). The observed increase in the catalytic activity with increasing HCOOH concentrations indicates differences in the rate determining step and/or a different HCOOH oxidation mechanism for low and high HCOOH concentrations. The results show that the anodic HCOOH oxidation reaction using Pt/WO_x anodes is more complicated than that suggested in Eq. (6).

3.2.3.1.2. $(COOH)_2$ oxidation. For the case of the $(COOH)_2$ oxidation, it was found that an increase in the $(COOH)_2$ concentration increases the magnitude of J even for low (10^{-3} M $COOH)_2$ concentrations, as shown in Table 6 using a 200 cm^2 real Pt area Pt/WO_x anode. The increase in J with the $(COOH)_2$ concentration (vs. the H_2SO_4 background solution) is seen to be less pronounced at more positive potentials. This is no surprise since the current of $(COOH)_2$ oxidation is essentially constant with potential and the current for parallel oxygen evolution is obviously increasing. However, the increase in J is sufficiently large throughout the potential region to indicate that these Pt/WO_x films are good anode catalysts for the $(COOH)_2$ oxidation reaction. Similar to the case of HCOOH electrolysis, the I_{eff} values for the $(COOH)_2$ at lower potentials (1.035 and 1.135 V) were larger than 100%, suggesting that $(COOH)_2$ is not oxidized to CO_2 under these particular conditions. In fact, it is likely that a poisoning (surface blocking) species is formed at the Pt/WO_x anode surface at these lower potentials, as was similarly observed for the HCOOH oxidation reaction. For this reason, reaction rate constants were not determined in the lower potential range (see Fig. 9). Fig. 9 shows the k_1 values

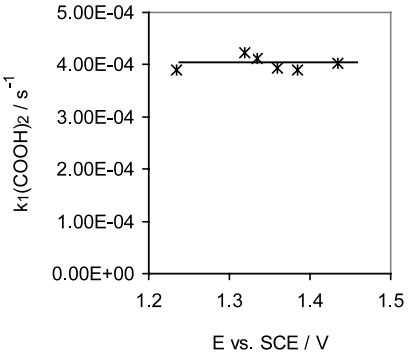

Fig. 9. Experimental k_1 values for the oxidation of originally 10^{-3} M $(COOH)_2$ + 0.5 M H_2SO_4 as a function of the applied potential. The k_1 values are extracted from experimental $\ln(c_0/c_{(t)})$ vs. time curves. The straight line indicates the best fit to the experimental data. A 200 cm^2 real Pt area Pt/WO_x anode of 0.98 cm^2 geometrical area was used for the electrolysis. The solutions were mechanically stirred.

determined for the oxidation of initially 10^{-3} M $(COOH)_2$ at different potentials above 1.135 V. It is seen that k_1 is independent of the potential. More careful studies carried out for the $(COOH)_2$ to CO_2 oxidation over short periods of time (thus maintaining the $(COOH)_2$ concentration within 10% of the initial value) also show no dependence of the rate on the applied potential. As mentioned above, careful studies of the influence of stirring rate and film thickness on the k_1 values carried out in parallel work suggest that the $(COOH)_2$ oxidation reaction is activation and not mass transport controlled [24]. The 1st order $(COOH)_2$ oxidation rate constant was also found to be independent of potential for thin (11 cm^2 real Pt) Pt/WO_x anodes where any mass transport limitations will be much less of a problem [24]. In accordance with these observations, the independence of the k_1 values on applied potential likely suggests that a chemical reaction of $(COOH)_2$ with the anode surface is involved in the overall oxidation reaction of $(COOH)_2$ to CO_2, and that this chemical reaction is the rate determining step. It is assumed that the carboxylic groups of the $(COOH)_2$ interact with the Pt/WO_x surface. The breaking of the

Table 6
$(COOH)_2$ influence on current density as a function of potential in 'mechanically stirred' solutions using Pt/WO_x anodes

E vs. SCE [a] (V)	$(J_{10^{-3}\ M\ (COOH)_2}/J_{0.5\ M\ H_2SO_4})$ [b]	$(J_{10^{-2}\ M\ (COOH)_2}/J_{0.5\ M\ H_2SO_4})$ [b]	I_{eff} [c] (%) c_0: 10^{-3} M $(COOH)_2$
1.035	180	1200	170
1.135	5	100	114
1.235	1.6	6.8	49
1.285	1.2	2.1	17.8
1.335	1.1	1.2	5
1.385	1.03	1.05	1.1

[a] The E values are recorded vs. an SCE, however, an MSE was used for the electrolysis experiments.
[b] The J values are extracted from experimental $J-t$ curves after 20 min of electrolysis at a particular potential. In all cases, the J value reached a pseudo steady-state within less than 20 min of electrolysis.
[c] The I_{eff} values are calculated from $(COOH)_2$ concentration changes observed during the anodic electrolysis carried out at a particular potential and using Eq. (9). The I_{eff} values reported in column 4 are for the $(COOH)_2$ concentration change of initially 10^{-3}–1×10^{-4} M.

carbon–carbon bond is possibly the rate determining chemical step in the $(COOH)_2$ oxidation reaction; this would explain the absence of the influence of potential on the reaction rate constant provided that the surface coverage of the organic is independent of potential.

4. Summary and conclusions

High surface area WO_x films containing foreign elements, namely Pt, Sn and Ru, were prepared via electrochemical deposition methods. All WO_x films showed high specific super-capacitive values of up to 180 F g^{-1} and rapid faradic film conversion reaction kinetics. The WO_x films formed by the co-deposition of Ru and Sn were found to exhibit close to ideal capacitive behavior. Initial life time studies showed that WO_x films containing Pt or Sn are stable when used as anodes in acidic solutions at 'high' currents; the films are also highly conductive. The Pt/WO_x anodes were found to oxidize a number of organics (aliphatic carboxylic acids and alcohols) at potentials more negative than needed for the O_2 evolution reaction, while only oxidation characteristics for $(COOH)_2$ were observed using Sn/WO_x electrodes. It is believed that the oxidation reaction carried out under these conditions involves the adsorption of the organic onto Pt sites, while the WO_x appears to mainly serve as a conductive backbone for the Pt sites that are involved in the organic oxidation reaction. Both Pt/WO_x and Sn/WO_x anodes were found to oxidize HCOOH and $(COOH)_2$ at more positive potentials at which O_2 is evolved, while neither CH_3COOH nor *t*-butanol were oxidized using Pt/WO_x or Sn/WO_x anodes in this potential range. Both the anodic oxidation reactions of HCOOH and $(COOH)_2$ carried out at sufficiently positive potentials appear to follow 1st order kinetics; higher current efficiencies were found for $(COOH)_2$ than HCOOH oxidation. Systematic HCOOH and $(COOH)_2$ electrolysis studies at positive constant potentials were carried out using Pt/WO_x anodes. The results suggest that adsorptive interactions of HCOOH and $(COOH)_2$ with the anode surface are involved in their oxidation reaction, with the potential determining the nature of the interaction. The reaction rate constants for $(COOH)_2$ oxidation are independent of the potential over a wide range.

Acknowledgements

The authors wish to thank Dr E. Gileadi (Tel-Aviv University, Isreal) and Dr Y. Kargin (Kazan State University, Russia) for helpful discussions. Assistance from P. L'Abbe (National Research Council Canada) for making the cells used in this work is also greatly acknowledged.

References

[1] B. Reichman, A.J. Bard, J. Electrochem. Soc. 126 (1979) 583.
[2] H.R. Zeller, H.U. Beyeler, Appl. Phys. 13 (1977) 231.
[3] M. Sun, N. Xu, Y.W. Cao, J.N. Yao, E.G. Wang, J. Mater. Res. 15 (2000) 927.
[4] M. Pourbaix, Atlas of Electrochemical Equilibria in Aqueous Solutions, 2nd ed., NACE International Cebelcor, Houston, Texas, USA, 1974, p. 280.
[5] R.J. Colton, A.M. Guzman, J.W. Rabalais, J. Appl. Phys. 49 (1978) 2778.
[6] D. Craigen, A. Mackintosh, J. Hickman, K. Colbow, J. Electrochem. Soc. 133 (1986) 1529.
[7] A. Chemseddine, R. Morineau, J. Livage, Solid State Ionics 9–10 (1983) 357.
[8] P.J. Kulesza, L.R. Faulkner, J. Electroanal. Chem. 248 (1988) 305.
[9] P.K. Shen, A.C.C. Tseung, J. Mater. Chem. 2 (1992) 1141.
[10] P.K. Shen, A.C.C. Tseung, J. Electrochem. Soc. 11 (1994) 3082.
[11] P.K. Shen, J. Syed-Bokhari, A.C.C. Tseung, J. Electrochem. Soc. 138 (1991) 2778.
[12] P.J. Kulesza, L.R. Faulkner, J. Am. Chem. Soc. 110 (1988) 4905.
[13] C. Bock, B. MacDougall, J. Electrochem. Soc. 146 (1999) 2925.
[14] B. Correa-Lozano, C. Comninellis, A. DeBattisti, J. Appl. Electrochem. 27 (1997) 970.
[15] P.G. Pickup, V.I. Birss, J. Electroanal. Chem. 240 (1988) 185.
[16] B.E. Conway, Electrochemical Supercapacitors: Scientific Fundamentals and Technological Applications, Kluwer Academic/Plenum Publishers, New York, 1999, p. 19.
[17] C. Bock, V.I. Birss, Electrochim. Acta 46 (2000) 837.
[18] R.D. Armstrong, J. Electroanal. Chem. 198 (1986) 177.
[19] C. Comninellis, Electrochim. Acta 39 (1994) 1857.
[20] A. Savall, Chimia 49 (1995) 23.
[21] J. Feng, L.L. Houk, D.C. Johnson, S.N. Lowery, J.J. Carey, J. Electrochem. Soc. 142 (1995) 3626.
[22] B.E. Conway, H. Angerstein-Kozlowska, Acc. Chem. Res. 14 (1981) 49.
[23] E. Gileadi, Electrode Kinetics for Chemists, Chemical Engineers, and Material Scientists, VCH Publishers Inc, New York, 1993, p. 140.
[24] C. Bock, A. Smith, B. MacDougall, Electrochim. Acta, submitted.
[25] Essays on Free-Radical Chemistry, special Publication 24, the Chemical Society Burlington House, London, 1970.